Quaternary Research

doi:10.1017/qua.2018.39

SPECIAL ISSUE

ALEUTIANS

Tsunami-based evidence for large eastern Aleutian slip during the 1957 earthquake

Frances R. Griswold[a], Breanyn T. MacInnes[b]*, Bretwood Higman[c]

[a]Department of Geosciences, University of Massachusetts Amherst, 627 N. Pleasant St., 233 Morrill Science Center, Amherst, Massachusetts 01003, USA
[b]Department of Geological Sciences, Central Washington University, 400 E. University Way, Ellensburg, Washington 98926-7418, USA
[c]Ground Truth Trekking, PO Box 164, Seldovia, Alaska 99663-0164, USA

(Received July 15, 2017; Accepted March 24, 2018)

Abstract

The Aleutian subduction zone is capable of generating magnitude ~9 earthquakes that have local impact and broadcast their destructive power across the Pacific through tsunamis. Field surveys of the tsunami from the 1957 Great Aleutian earthquake (reported M_w 8.6) indicate a tsunami amongst the largest of the twentieth century. In the eastern half of the rupture zone, stranded logs record up to 18 m run-up in the Islands of Four Mountains (IFM) and 32 ± 2 m on Unalaska Island. In conjunction with archaeological studies in the region, these observations show the potential impact of tsunamis on the ancient peoples in the IFM. Simulation of the near-field tsunami produced from the published slip distribution of 1957 is almost an order of magnitude smaller than all field observations. Increasing the earthquake magnitude and amount of eastern slip used in forward models of the tsunami demonstrate that run-up observations can be achieved throughout the eastern Aleutians if the earthquake was more than twice as large—at least M_w 8.8 earthquake with 10–20 m of eastern slip. Additionally, up to five possible IFM paleotsunami deposits agree with the regional picture of regular large events, illustrating the circum-Pacific tsunami hazard from the east-central Aleutians.

Keywords: Tsunami; Tsunami modeling; 1957 Aleutian earthquake

INTRODUCTION

The Aleutian subduction zone is oriented such that earthquake tsunamis from there pose a threat throughout the Pacific Ocean. However, the seismic history and associated tsunamis of the Aleutian Islands are relatively unstudied. The eastern Aleutian Islands are of particular interest to the United States because tsunamis from this area of the subduction zone can affect both Hawai'i and the west coast of North America. For example, the 1946 earthquake and tsunami (Fig. 1) destroyed infrastructure in Alaska, and Hawai'i sustained 26 million (1946) dollars in damage (National Oceanographic and Atmospheric Administration [NOAA], National Geophysical Data Center [NGDC], 2017). The 1957 earthquake and tsunami (Fig. 1) caused 5 million (1957) dollars damage in Hawai'i (Strover and Coffman, 1993), where two villages were destroyed; caused minor damage in San Diego Bay, California; and affected Chile, Japan, and El Salvador (NOAA, NGDC, 2017).

In addition to trans-Pacific effects, the near-field hazard of eastern Aleutian tsunamis affected local maritime Aleut peoples who occupied the region for at least 8500 yr (Black, 1974; Laughlin et al., 1975; Aigner, 1977). Assessing the degree to which tsunami inundation disrupted human and ecological systems can help reveal the ecodynamics involved in the westward human settlement of the Aleutians and the development of prehistoric human adaptations to tsunamis. These are important lessons for current inhabitants of the northern Pacific Rim.

Whether interested in the future or the past, near-field or trans-Pacific, the key variables in defining the tsunami hazard are the size and frequency of earthquakes and tsunamis in the eastern Aleutian archipelago (cf. Butler et al., 2016). This study contributes new field observations of the 1957 tsunami and paleotsunamis in the Islands of Four Mountains (IFM) and Unalaska Island in the eastern section of the aftershock zone of the 1957 earthquake (Fig. 1). Field investigations included mapping inundation and run-up from wrack-line locations and geomorphic observations of the tsunami, and tracing tsunami deposits when present. Combining the new

*Corresponding author at: Department of Geological Sciences, Central Washington University, 400 E. University Way, Ellensburg, Washington 98926-7418, USA. E-mail address: macinnes@geology.cwu.edu (B.T. MacInnes).

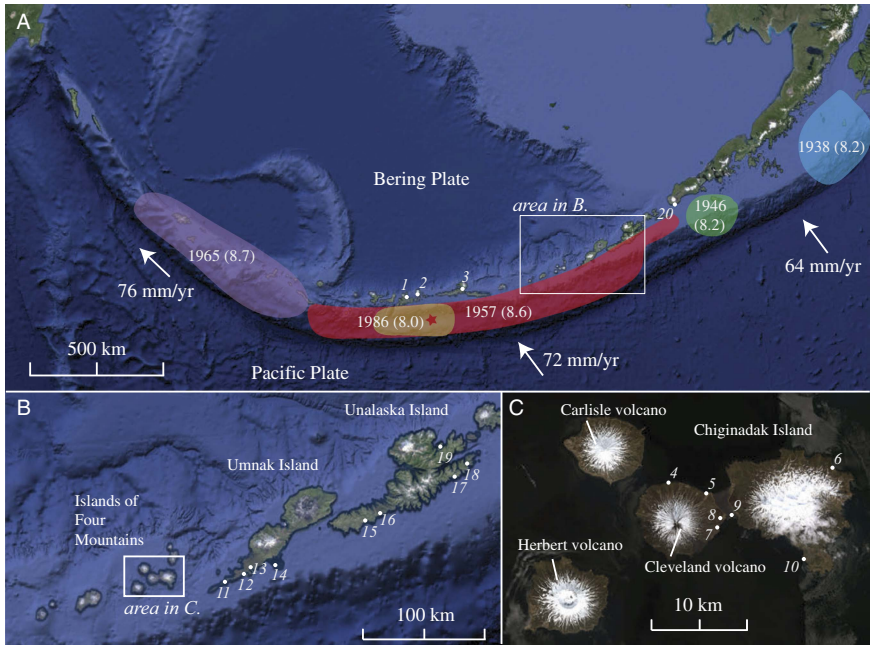

Figure 1. (A) Map of the Aleutian Island arc. Ovals denote aftershock zones of major historical Aleutian earthquakes, M_w in parentheses; modified from Wesson et al. (2007). Star denotes 1957 epicenter. White dots and italic numbers refer to site locations in Table 1. Rate of convergence from DeMets et al. (2010). Image from Google Earth. (B and C) Maps and place names for the area of this study. Images from Google Earth (B) and WorldView (C). (For interpretation of the references to color in this figure legend, the reader is referred to the web version of this article.)

field observations with ongoing work of the U.S. Geological Survey (USGS) in the area (Witter et al., 2014, 2016) and eyewitness accounts from 1957 (Lander, 1996) creates a suite of 19 observations covering much of the rupture area (Table 1). By comparing these observations with simulations using GeoClaw, an open-source tsunami model (Mandli et al., 2016), we independently concur with the estimates of Witter et al. (2016) and Nicolsky et al. (2016) of extensive slip in the 1957 rupture eastern extent from a higher-magnitude earthquake than the cataloged value.

BACKGROUND

The eastern-central Aleutian subduction zone

The volcanic arc of the Aleutian Islands is located where the Pacific plate is subducting beneath the Bering plate. In the east-central Aleutians, this occurs at a rate of ~70 mm/yr (Cross and Freymueller, 2008; DeMets et al., 2010; Fig. 1). Five major earthquakes in the past century, the 1938 Alaskan, 1946 Aleutian, 1957 Aleutian, 1964 Prince William Sound, and 1965 Rat Islands earthquakes have collectively ruptured nearly the entire length of the Aleutian arc (Fig. 1). In the east-central Aleutians, geodetic studies indicate that the subduction zone off Umnak Island and much of Unalaska Island is partially locked; however, the eastern end of Unalaska is currently creeping, and the west of Umnak and the IFM is unknown (Freymueller et al., 2008).

Past events in the east-central Aleutians are known from paleotsunamis on Sedanka Island and the island of Kaua'i, Hawai'i. Six paleotsunami deposits in the past 1700 yr at Stardust Bay, Sedanka Island, indicate a recurrence of every 300–340 yr (Witter et al., 2016). A paleotsunami younger than 525–285 cal yr BP preserved in a sinkhole on the island of Kaua'i is estimated to have been generated by a tsunami from a M_w 9.25 earthquake from the eastern Aleutians (Butler et al., 2014).

The 1957 Great Aleutian earthquake parameters

The 1957 Great Aleutian earthquake occurred March 9, 1957, at 14:22:31.9 GMT (NOAA, NGDC, 2017). Solutions of the seismic moment are disputed (Oliver and Murphy, 1971; Peterson and Hutt, 2014; Nicolsky et al., 2016), but magnitude estimates range from M_w 8.3 (Sykes et al., 1980) to M_w 9.1 (Kanamori, 1977) based on the aftershock area; M_w 8.6 is the currently accepted value for the NGDC. However, a M_t (tsunami magnitude; Abe, 1979) value of 9.0 is high compared with the earthquake magnitude. The epicenter was south of Atka Island, and the rupture extended ~350 km west and ~850 km east (Fig. 1), crossing from the central Aleutians into the eastern Aleutians. Herein we define the eastern part of this rupture zone as from the IFM to the east side of Unalaska Island.

A detailed slip distribution of the 1957 rupture is difficult to constrain because sparse records are available. Johnson et al. (1994) calculated parameters of a source model from far-field tsunami tide-gauge observations and seismic-wave studies and concluded that the majority of the slip occurred in the western part of the aftershock zone with virtually no slip occurring in the eastern half. Recent work combining tsunami observations with modeling of Johnson et al.'s (1994) source model to

https://doi.org/10.1017/qua.2018.39 Published online by Cambridge University Press

Table 1. Tsunami wrack-line surveys (this study), geologic surveys, and historical accounts of the 1957 Aleutian tsunami run-up and inundation. Locations in italic are estimated positions based on descriptions. Numbers 12, 14, 15, and 17 and the unnumbered rows were not used to validate tsunami simulations.

No. in Figure 1	Location	Island	Reference	Latitude (°N)	Longitude (°W)	Run-up (m)	Inundation (m)	Notes
1	Sweeper Cove	Adak	Lander (1996)	*51.863*	*−176.62*	~3.8	-	"Rise in water of 12.5 ft."
2	Sand Bay	Great Sitkin	Lander (1996)	*51.98*	*−176.09*	~4	-	All structures below 13 ft. destroyed, wave maybe up to 26 ft.
3	Nazan Cove	Atka	Lander (1996)	*52.22*	*−174.19*	~9	-	Pilings washed to a height of 30 ft. in Atka Harbor
4	North Cleveland	Chuginadak	This study	52.8592	−169.9599	9.0	80	Wrack line; traces out a "splash" shape
5	West Applegate Cove	Chuginadak	This study	52.8511	−169.8942	6.7	65	Wrack line
6	Corwin Rock Cove	Chuginadak	This study	52.8736	−169.7014	7.3	70	Wrack line
7	Southeast Cleveland	Chuginadak	This study	52.8189	−169.8829	14.9	195	Wrack line
8	South Cove	Chuginadak	This study	52.8279	−169.8785	>13.0	560	Tsunami deposit and driftwood; tsunami inundated to back cliff and reflected
9	South Cove Isthmus	Chuginadak	This study	52.8333	−169.8656	15.3	690	Wrack line
10	Concord Point	Chuginadak	This study	52.7899	−169.7476	17.6	165	Wrack line; traces out a "splash" shape
11	Cape Sagak	Umnak	Black (1974)	*52.83*	*−169.08*	>10 m	Overtopped cape	Completely overtopped cape (elevation of cape reported as 10 m)
12	Ogalodagh	Umnak	Black (1975)	*52.91*	*−168.86*	-	-	Bay was "overrun"
13	Driftwood Bay	Umnak	Black (1975); Witter et al. (2014)	52.9512	−168.7858	23	~200	Stranded driftwood logs
14	Trapper's Cove	Vsevidof	Lander (1996)	*52.98*	*−168.48*	-	-	Four sheep camps washed away
	the "Pacific coast"	Umnak	Lander (1996)	-	-	~12–14	~400	No location given; generally, driftwood moved to "40–45 ft. high and 1/4 mile inland"
	the "Pacific coast"	Umnak	Lander (1996)	-	-	~23	-	No location given; report from Umnak resident
15	Huddle Rock Bay	Unalaska	This study	53.3363	−167.4005	22 ± 3	70	Isolated driftwood
16	East of Riding Cove	Unalaska	This study	53.392	−167.232	32 ± 2	800	Wrack line
17	Unnamed bay	Unalaska	This study	53.687	−166.346	>10 m	>600 m	Sand-boulder deposit
18	Stardust Bay	Sedanka	Witter et al. (2015)	53.7740	−166.2077	18.5	800	Driftwood logs and deposit
19	Dutch Harbor	Unalaska	Johnson et al. (1994)	53.898	−166.515	0.69	n/a	Tide gauge
20	Scotch Cap	Unimak	Lander (1996)	*54.402*	*−164.794*	~12	-	Lighthouse personnel report wave up to 40 ft.
21	Hanalei	Kaua'i , Hawai'i	NOAA, NGDC (2017)	22.216	−159.501	5.8	n/a	Post-tsunami survey measurement
22	Anahola	Kaua'i , Hawai'i	NOAA, NGDC (2017)	22.150	−159.303	4.9	n/a	Post-tsunami survey measurement

Stardust Bay and Dutch Harbor conclude that this solution is missing large seafloor displacement (estimated as slip at least 10 m at depths shallower than 30 km) offshore of Unalaska and Sedanka Islands (Nicolsky et al., 2016; Witter et al., 2016).

Observations of the 1957 tsunami

The 1957 tsunami was registered at more than 150 tide gauges and has 326 run-up observations throughout the Pacific Ocean (NOAA, NGDC, 2017). Sites relevant to this study are summarized in Table 1. At the western end of the 1957 rupture area, reports from the protected sites of Sweeper's Cove on Adak Island suggest a rise in water of 3.8 m. In Sand Bay on Great Sitkin Island, all structures below ~4 m were destroyed, and one report of an ~8 m wave exists (Lander, 1996). In Nazan Bay, the main harbor on Atka Island, pilings were washed up to a height of 9 m (Lander, 1996).

Eyewitness accounts in the eastern 1957 rupture area include Trapper's Cove on Vsevidof Island (an island off the southwest coast of Umnak Island) where four sheep camps were washed away (Lander, 1996) from a wave with reportedly 13.7 m run-up (NOAA, NGDC, 2017). Black (1974, 1975) reports that many low-lying sites on Umnak Island, including Cape Sagak, Ogalodagh, and Driftwood, were all "overrun" by the tsunami; the tsunami completely overtopped the western tip of Umnak Island, which sits at ~10 m elevation. Lander (1996) reports that along the Pacific coast of Umnak, driftwood was washed about 400 m inland and generally to ~12–14 m elevation, but as high as 23 m; no specific locations are given. At the western end of Unimak Island, east of the rupture area, Scotch Cap lighthouse personnel reported the tsunami at 12 m. Finally, a tide gauge measurement of the tsunami from protected east-facing Dutch Harbor on Unalaska Island recorded 0.69 m with a positive first wave arrival (Salsman, 1959; Nicolsky et al., 2016; NOAA, NGDC, 2017).

Field research on the 1957 tsunami at Umnak and Sedanka Islands used ^{137}Cs dating methods to identify wrack lines and tsunami deposits as occurring from the 1957 tsunami. The results indicate 23 m run-up in Driftwood Bay, Umnak Island (Witter et al., 2014), and 18.5 m run-up in Stardust Bay, Sedanka Island (Witter et al., 2016).

Far-field observations of the 1957 tsunami include tsunami deposits, eyewitness accounts, and post-tsunami survey data from throughout the Pacific (NOAA, NGDC, 2017). The tsunami inundated throughout the Hawai'ian Islands, including in particular for this study, Anahola, Kaua'i, on the northeastern side of the island (4.9 m) and Hanalei on the north shore of Kaua'i (5.8 m) (Griswold et al., 2016; La Selle et al., 2016; NOAA, NGDC, 2017).

TSUNAMI WRACK LINES AND DEPOSITS

Field methods

Field observations in the IFM were collected in 2014 by MacInnes and Griswold during the interdisciplinary project "Prehistoric Resilience in the Islands of Four Mountains" and observations on Unalaska by Higman in 2015. Site selection in the IFM included using satellite images to locate low-lying coastal areas, aerial reconnaissance via helicopter, and word-of-mouth reports of possible wrack lines. Sites on Unalaska were encountered along the walking and paddling route of Higman from Nikolski to Dutch Harbor.

Geologically, tsunami inundation is identified through two primary depositional features on land: a wrack line and a sediment deposit. Wrack lines are continuous lines of floatable driftwood and debris that record the farthest inland distance water traveled during the tsunami. Inundation is the maximum horizontal distance from the ocean that was flooded by a tsunami, and run-up is the elevation above mean sea level of the inundation point (International Tsunami Survey Team [ITST], 2014).

Most tsunami surveys involving wrack lines are conducted soon after the event; this study is unusual because the wrack line was 57 yr old at the time of measurement. In most places in the world, a wrack line is ephemeral because of human land-use practices, soil forming processes, or decomposition. However, the Aleutian Islands provide a location where tsunami survey methodology (ITST, 2014) can be applied to much older events because driftwood decomposition and burial rates are suppressed by climate and ecology. As such, the main difference between the tsunami survey methodology used here and that of modern tsunami surveys is the lack of eyewitness interviews. Because there are no trees in the Aleutians, every log found in a wrack line was originally driftwood.

Distinguishing tsunami from storm wrack lines and estimating the timing of deposition entailed using the following criteria. Based on these criteria, we determined that some locations did not definitively contain a 1957 wrack line.

1. *Vegetation cover and decomposition*: The vegetation covering and decomposition rate of logs can vary from site to site related to local climatic and biotic conditions. However, regardless of location, all logs within the same site deposited at the same time should indicate similar degrees of decomposition.
2. *Inland position:* Wrack lines should run roughly parallel to the current beach and storm ridge. The lateral distance between the wrack lines and the shoreline provides additional supporting evidence. Storm waves have short inland penetration (cf. Morton et al., 2007); thus storm wrack lines are closer to the modern shore position. If logs lie significantly beyond the modern beach, log deposition is more likely from tsunamis.
3. *Date of manufacture:* Wrack lines associated with the 1957 tsunami should contain only material manufactured before 1957, such as buoys, metal, and glass, with the possible exceptions of surficial debris light enough to become airborne in strong winds, such as Styrofoam and pieces of light plastic. The same amount of vegetation would not cover these lighter items as the driftwood logs and debris associated with the tsunami.

To calculate elevation and inland position of wrack lines at the IFM sites, we measured topographic transects with a

https://doi.org/10.1017/qua.2018.39 Published online by Cambridge University Press

transit level and rod from sea level to the wrack line at each site and traced the wrack line perpendicular to the transect. Wrack-line elevation measurements are not necessarily identical along the trace of the wrack line because of variations in topography, wave intensities, and geomorphology of the coastline. We reported the highest point of the wrack line as the official run-up for each location in Table 1.

Each transect experienced variable degrees of error based on visibility and weather conditions; cumulative error during fair weather conditions averaged 0.63 mm in elevation and 125 mm horizontal distance, and during poor weather conditions (transects Southeast Cleveland, Isthmus, Concord Point, South Cove, and West Applegate) averaged 4.2 mm in elevation and 840 mm horizontal distance. Elevations were corrected for tides using verified water-level data from the nearby Nikolski tide gauge; corrections ranged from –0.3 to –0.47 m (NOAA, 2017). No correction was made for the tide at the time of the tsunami.

The two new Unalaska wrack-line positions (Table 1), at Huddle Rock Bay and east of Riding Cove, were noted with a hand-held GPS, then later analyzed to determine elevation and distance inland using Google Earth, USGS topographic maps, and ArcticDEMs, which were created from DigitalGlobe Inc. imagery and funded under National Science Foundation awards 1043681, 1559691, and 1542736. The error associated with these two sites is based on the position error of the GPS location of the logs overlaid on the digital elevation model (DEM). In addition to the new Unalaska wrack-line sites, the near-surficial tsunami deposit was documented at an unnamed bay (site 17 in Table 1).

In the IFM, the coastal plain at South Cove preserves buried sand sheets indicative of paleotsunamis. We measured two topographic profiles and described the stratigraphy of 11 excavations. Tsunami deposits were identified as clean black/gray sand of similarly mixed mineral composition as beach sand sediment. Lahars were identified as poorly sorted silty gravel to boulders, many of which were angular (Supplementary Fig. 1). We also sampled soil for radiocarbon and sand for optically stimulated luminescence dating, but none of these samples were able to ultimately provide viable dates.

Field results: run-up and inundation

Soil development and log burial in wrack lines varied site to site, ranging from no burial to partial burial to complete burial by assorted meadow grasses and lichen, crowberries (*Empetrum nigrum*), and peat moss (*Sphagnum* sp.) (Fig. 2). Sections of exposed driftwood were often waterlogged and falling apart. In contrast, newer logs from recent large storms were still solid, and it was difficult to manually break them apart (Fig. 2). No debris found in the wrack lines indicated post-1957 manufacture, except a few empty plastic bottles lying on the surface. Old orange and metal buoys could be found in most wrack lines (Fig. 2), whereas other, more modern types of buoys were not. Concord Point in particular had several old orange buoys that were covered or buried comparable to the driftwood logs in the wrack line and had been chewed extensively by foxes (*Vulpes vulpes*). Although we were unable to determine the exact date of when these orange buoys were first used, discussions with members of the Puget Sound Maritime Historical Society indicate they were in use during 1950s.

Wrack-line measurements show tsunami run-up was higher on the Pacific side sites than on the Bering side (Table 1, Fig. 1), as expected for a subduction-zone earthquake. Highest observed run-up was east of Riding Cove (32 ± 2 m), followed by Driftwood Bay (23 m) (Witter et al., 2014), Stardust Bay (18.5 m) (Witter et al., 2016), and Concord Point (18 m). South Cove lacked a wrack line, but scattered logs and tsunami deposit studies indicated the wave reached at least 13 m high at the cliff at the distal end of the cove. Run-up on the Bering side of the IFM ranged from 7 to 9 m with a maximum at North Cleveland (Table 1). Although limited by the number of sites in this study, Pacific-side run-up appears to be higher overall in Umnak, Unalaska, and Sedanka Islands than in the IFM (Table 1).

At two sites, Concord Point and West Applegate Cove, the wrack line traced out a continuous arc centered around slight embayments in the coastline, with the highest elevation at the apex of the curve. Concord Point is a steep bedrock slope, and West Applegate Cove a steep erosional scarp. Our interpretation is that the shape of the coast combined with the steep slope caused focusing and created a locally enhanced "splash" of the tsunami at these sites.

Field results: tsunami deposits

A clean sand deposit with an erosional base ~10 cm below the surface extended continuously to the back of the coastal plain in South Cove (Fig. 3). Sediment composition mirrored the sandy beach of the nearby isthmus; the modern proximal beach was composed of cobbles and boulders, and a grab sample of offshore sediment was finer grained, with a higher concentration of heavy minerals. We interpreted the upper deposit as being from 1957 based on its stratigraphic location below a tephra field—identified as being from the 2001 Cleveland eruption. The deposit does not exhibit the inland thinning often associated with tsunami deposits, but rather thickens at the landward extreme (Fig. 3), potentially because of reflection off the cliff at the distal end of the coastal plain (Higman, 2007).

Similar clean sand deposits were found intercalated with soils, lahars, and other sands in excavations in the back northwest corner of South Cove. Although these deposits are difficult to correlate, at most five such deposits are visible in excavation 209, three interpreted as paleotsunamis with confidence, and one to four were present in other excavations (Fig. 3). These sand layers are interpreted to be paleotsunami deposits based on lack of soil development and their composition and grain-size similarities with the 1957 deposit and beach samples. Additionally, similar deposits were not present in upland sites overlooking South Cove at elevations higher than tsunamis typically inundate.

At a nameless bay along eastern Unalaska Island, a likely tsunami deposit and possible tsunami scour features suggest

https://doi.org/10.1017/qua.2018.39 Published online by Cambridge University Press

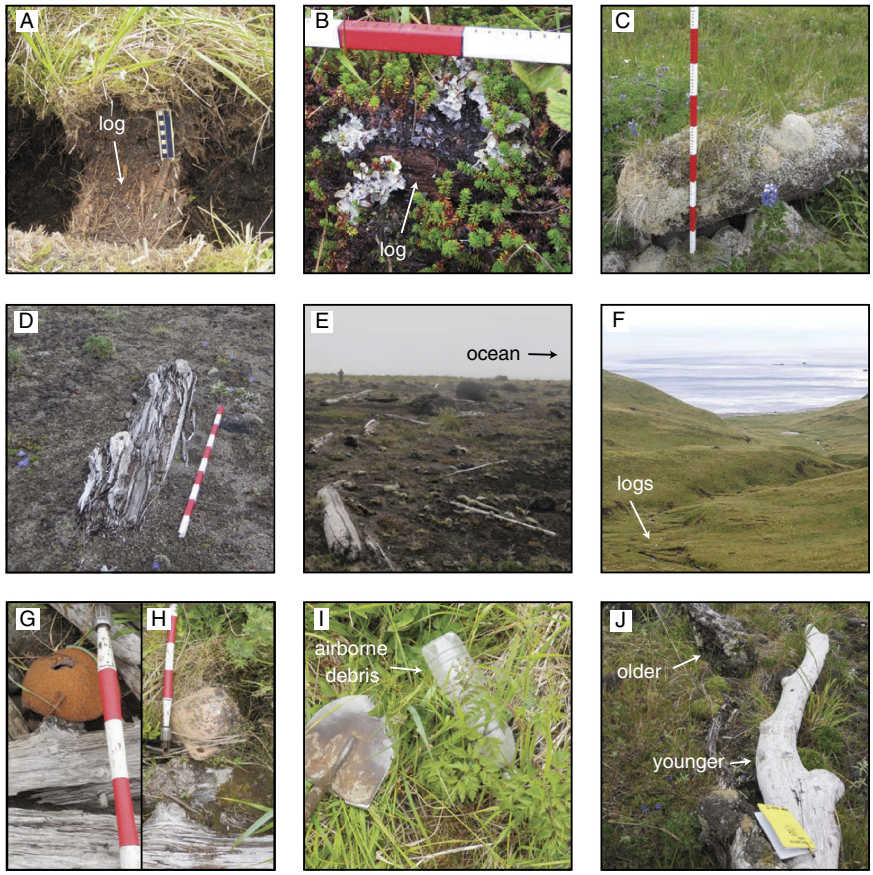

Figure 2. (color online) Example pictures. (A) Complete burial in meadow vegetation of a wrack-line log (log dug out); scale is 10 cm, with 1 cm increments. (B) Partial burial in tundra; scale's upper tick marks are in centimeters. (C) Partial burial in meadow vegetation and lichen; measuring stick is painted in 10 cm increments. (D) No vegetation cover; logs are decomposing. (E) Wrack line (at Southeast Cleveland), person for scale. (F) Wrack line at east of Riding Cove. (G and H) Metal and orange buoys, respectively; scale interval is 10 cm. (I) Example of airborne debris with shovel head for scale. (J) Juxtaposition of younger and older logs together, indicative of a storm wrack line; field book is 17.5 × 11.5 cm.

the 1957 tsunami was large in this area as well. Near 53°41.22'N, 166°20.76'W, sediment ranging from sand to 2 m diameter boulders was scattered hundreds of meters across a beach plain and small hill into a lake (Supplementary Figs. 2 and 3). The deposit is interpreted as the 1957 tsunami deposit because it is very recent (lightly vegetated), does not exhibit geomorphic forms typical of normal beach processes, and no other process would comingle angular cobbles and boulders derived from the hill with rounded cobbles and boulders from the beach (Supplementary Fig. 2). Though this deposit only vaguely constrains the size of the tsunami here, the large boulders in it suggest a strong flow at least several meters deep over the beach berm, and the angular fragments of bedrock from the hill show the wave exceeded beach plain elevations with a flow strong enough to entrain these clasts. Finally, the deposit was quite thick—the base was not reached after 25 cm of trenching in two locations. Sandy subduction-zone tsunami deposits are usually thinner than 25 cm, and thicker deposits are typically associated with >5 m flow depths (Goto et al., 2014). Given the beach berm height of about 5 m above mean sea level, this implies run-up over 10 m. Though this deposit occurs only at this bay, it is associated with tsunami-caused shore-parallel scour features (Supplementary Figs. 1B and 4) that are also seen elsewhere on Unalaska at 53°41.326'N, 166°22.62'W and 53°41.304'N, 166°22.71'W and can be seen on satellite imagery available through Google Earth farther west near 53°37.2'N, 166° 33.6'W (Supplementary Fig. 4).

Field results: coastal natural hazards

The geomorphology and stratigraphy of South Cove revealed a geologic history of a coastal plain controlled by local natural hazards. Lahars immediately west of South Cove and numerous lahars within the stratigraphy of South Cove (Figs. 3 and 4) give evidence of sudden impulses of sediment to the system. Young beach ridges, angled at 45° to the present beach and sandwiched between the modern beach ridge and an older beach ridge (Fig. 4) are indicative of rapid formation. Recent large eruptions from Cleveland, such as the 2001 and 1944 eruptions (Global Volcanism Program, Smithsonian Institution, 2013), are likely the source of new sediment to the coastal zone. Rapid shoreline changes attributable to sudden increased sediment loads are common on island coastlines

https://doi.org/10.1017/qua.2018.39 Published online by Cambridge University Press

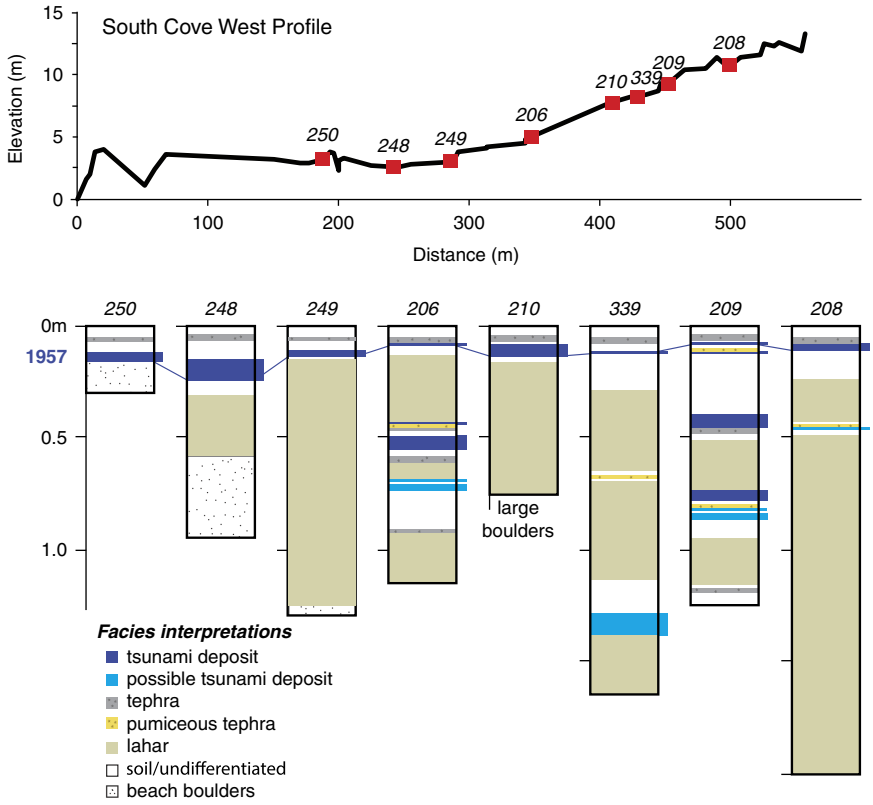

Figure 3. (color online) Topographic profile and excavations of the western transect in South Cove on Chuginadak Island. The upper tsunami deposit is interpreted as from the 1957 Aleutian tsunami. Correlation of paleotsunami deposits is challenging because of the interfingering of lahar deposits sourced from the volcano above. See Figure 4 for transect and excavation locations.

from volcanic eruptions (Major et al., 2000; Scott et al., 2010; Ramalho et al., 2013).

Rapid shoreline change is further reflected in the stratigraphy within South Cove. Excavations seaward of 300 m showed thin sediment cover over beach boulders while excavations landward of 300 m contain numerous depositional events (Fig. 3). This dramatic change of stratigraphic cover isolates an abrupt juxtaposition of age, showing recent

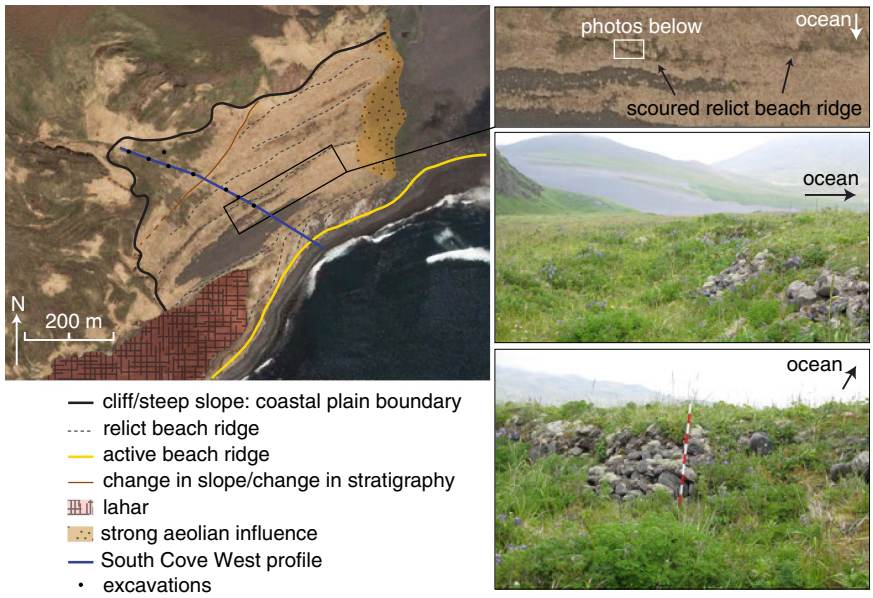

Figure 4. (color online) Map of South Cove geomorphology; image from Digital Globe. The change in slope at 300 m inland that corresponds to a change in stratigraphy is noted. The three images on the right show scours into the landward side of a relict beach ridge: the upper image is a satellite view (image from WorldView). The measuring stick is 1 m high.

https://doi.org/10.1017/qua.2018.39 Published online by Cambridge University Press

progradation. The location represents either a prolonged paleoshoreline or an erosional scarp from maximum transgression, with a relative age between the 1957 tsunami and the penultimate tsunami deposit. An important implication of this is that paleotsunami inundation distances cannot be known because the associated shoreline position is either not identifiable or not preserved.

Tsunami inundation has altered the surficial geomorphology of South Cove through erosion. Surficial scours into the landward side of relict beach ridges lay throughout the coastal plain (Fig. 4). Scours are defined by an area of missing stratigraphic cover where only bare boulders are exposed. Lichen growth on the exposed boulders was comparable to the growth on nonorganic material in 1957 wrack lines and covered greater areas than boulders associated with the modern beach ridge. The scour sides were steep on the seaward edge and shallow landward, with the deepest part on the seaward end (Fig. 4). These features are interpreted as being formed from tsunami inflow as it accelerated over the beach ridge (as in Kitamura et al., 1961; MacInnes et al., 2009).

TSUNAMI MODELING

Modeling methods

With the combined wrack line and eyewitness accounts (Table 1) as a validation tool, we investigated characteristics of the 1957 earthquake rupture using the tsunami model GeoClaw version 5.3.0 (Clawpack Development Team, 2014). GeoClaw solves the two-dimensional, shallow-water wave equations using a finite volume method (Berger et al., 2011; Mandli et al., 2016) to propagate tsunamis from seafloor deformation. GeoClaw is an open-source software package that is approved by the United States National Tsunami Program for the modeling of tsunamis (LeVeque et al., 2011). Inundation is fully integrated into the code. The depth-averaged nonlinear equations in GeoClaw show good agreement to validation studies, although as with any shallow-water wave tsunami model, the code only approximates the dynamics of wave breaking and overland flow (LeVeque et al., 2011).

Required inputs for GeoClaw simulations are bathymetric and topographic data sets and earthquake parameters to create seafloor deformation. Instantaneous seafloor deformation is calculated from slip on a fault, or multiple faults, using the Okada (1985) equations. Available bathymetric data sets are low resolution in the Aleutians field area: the Small Southern Alaska (SAK) bathymetry (Lim et al., 2011) is 24 arc-seconds, and the ETOPO1 Global Relief Model (Amante and Eakins, 2009) is 30 arc-seconds. We subdivided these grids in GeoClaw into 4 arc-seconds to allow for more robust representation of tsunami wave dynamics during simulation. Hawai‘i sites used high-resolution bathymetry cut from a 1/3 arc-second DEM of Kaua‘i (Friday et al., 2012) and ETOPO1 to cross the Pacific.

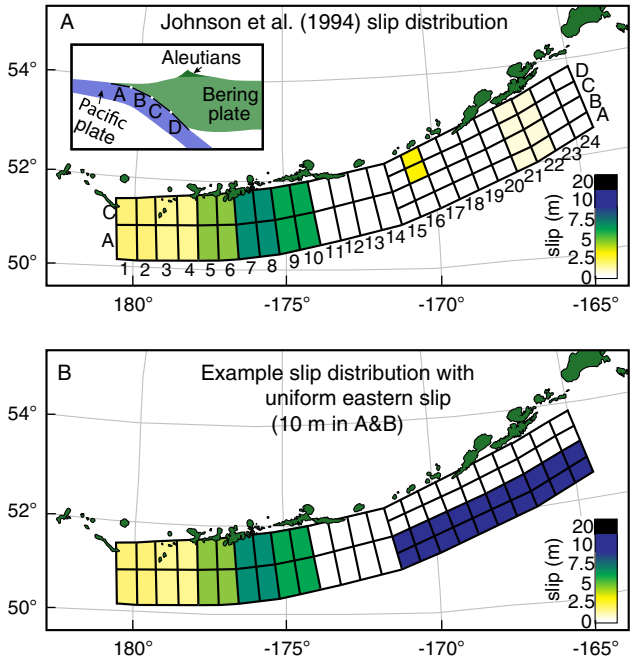

Figure 5. (color online) (A) Subfault geometry used in this study, populated with the values for the slip distribution by Johnson et al. (1994). Inset shows a cross section through the subduction zone, with progressively deeper subfaults labeled A–D. (B) Example of a hypothetical slip distribution used in this study. Only subfaults 15–24, A–D were manipulated in hypothetical cases.

We created source models by varying slip on a subfault grid that divided the subduction zone into 24 × 2 subfaults in the western half and 24 × 4 subfaults in the eastern half of the rupture (Fig. 5; Supplementary Table 1). The locations of each subfault are originally based on those used by Johnson et al. (1994), with one additional row of subfaults at the eastern end. The geometry for the strike and dip of the subduction-zone interface is from Slab1 (Hayes et al., 2012). We held the rake constant at 90° because the eastern Aleutians have nearly arc-normal subduction (Johnson et al., 1994). Of note, there is overlap in subfaults 14C and 14D with 15C and 15D immediately west of the IFM (Fig. 5) because of a change in strike. However, the problem of a local doubling of slip in that location because of the overlap was not an issue because no source models had slip in row 14.

Forward-modeling techniques inherently result in a suite of possible solutions; thus our aim in comparing simulation results to field observations is to refine general characteristics of the 1957 rupture. To evaluate models, we used four methods: the difference between simulation and observation in meters, the percent difference at each site, the root-mean-square (RMS) of the percent differences, and a count of the number of sites with a percent difference between –25% and +25%. We calculated the percent difference by subtracting the observed run-up from simulated at each site and dividing by observed. We subdivided percent differences at intervals of ± 25%, ±25% to ±50%, and more than ±50%. These

https://doi.org/10.1017/qua.2018.39 Published online by Cambridge University Press

calculations directly determine if simulated run-up was too high or too low, which can be used to compare spatial patterns. When evaluating sites, we focused more on sites with post-tsunami survey observations rather than eyewitness accounts because post-tsunami surveys provide more reliable observations. In general, we also ignored sites where all models were routinely underestimated, possible reasons for which we discuss below.

Modeling results: Johnson et al. (1994) source model

Simulations of the source model from Johnson et al.'s (1994) solution did not produce run-up close to the observed values at any site (Fig. 6; Supplementary Table 2). At the three eyewitness locations in the western part of the rupture zone (sites 1–3), simulated run-up was all less than 2 m, with simulated run-up at the Nazan Bay site 93% too small. Highest simulated run-up values in the eastern part of the rupture were 1.3 m at the Isthmus site in the IFM and 1.6 m east of Riding Cove, with percent differences ranging from 88% to 100% too small for each (Fig. 6). No run-up was produced at Scotch Cap, where observers documented water reaching 12 m high. These results are similar to those obtained by Witter et al. (2016) who modeled a tsunami from Johnson et al.'s (1994) source as not overtopping the beach berm in Stardust Bay where observed run-up was 18.5 m. Our results at Stardust showed a wave only 0.5 m high.

Because Johnson et al.'s (1994) preferred solution included isolated 3.3 m slip on subfaults 15C and 15D near the IFM, we also modeled a few variations of that isolated slip.

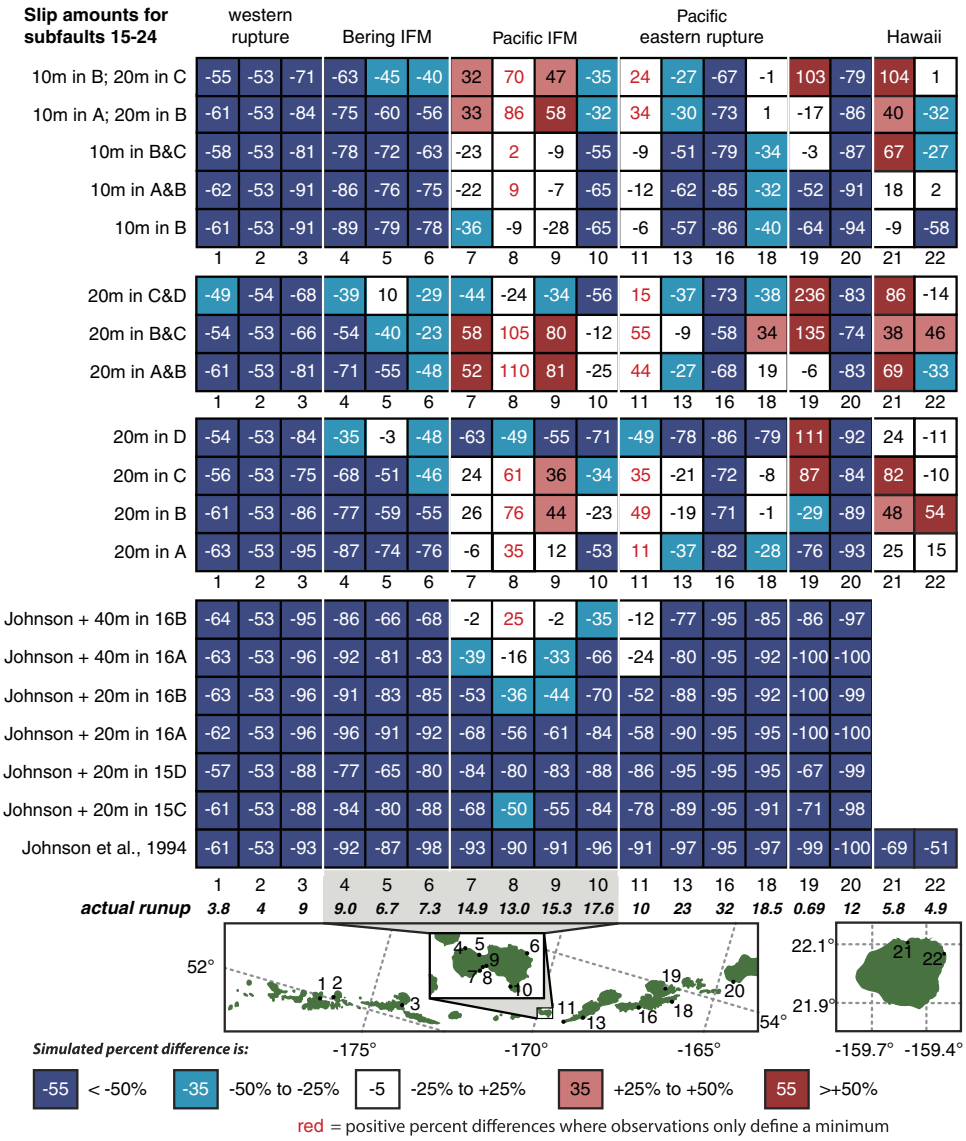

Figure 6. Tsunami simulation comparison to observations organized by source model. Numbers in colored boxes indicate the calculated percent difference between observation and simulation. Negative (blue) boxes are smaller simulated run-up than observed by ±25%, and red boxes are larger than ±25%. Subfault numbers for each source model can be found in Figure 5, and site location numbers can be found in Table 1 and Figure 1. IFM, Islands of Four Mountains. (For interpretation of the references to color in this figure legend, the reader is referred to the web version of this article.)

https://doi.org/10.1017/qua.2018.39 Published online by Cambridge University Press

These variations included increasing the 3.3 m slip to 20 m on subfaults 15C or 15D, as well as 20 and 40 m on the shallow subfaults 16A or 16B, directly offshore of the IFM (M_w 8.67 and 8.7, respectively). All of these modifications can be considered slight modifications to Johnson et al.'s (1994) solution, or they could represent a possible local submarine landslide associated with the earthquake. The 20 m slip simulations slightly improved results in the IFM and Umnak, while the 40 m slip simulations were within or close to within ± 25% (Fig. 6). However, outside of the IFM and western Umnak Island, the results remained roughly similar to the original Johnson et al. (1994) source simulation (Fig. 6), and thus localized extreme slip near IFM fails to reproduce our observations.

Modeling results: new earthquake source models

Clearly, greater tsunami excitation than was suggested by Johnson et al. (1994) is necessary in the eastern half of the rupture zone. Our straightforward approach to increasing tsunami run-up was to add uniform slip along the subduction zone in the eastern portion of rupture, with slip varying along dip but not along strike (Fig. 5). Standard deviation of results on the western side of the rupture remained less than 10% from the original Johnson et al. (1994) source model. We set slip in the east at either 10 or 20 m along a swath one or two subfaults wide, resulting in source model M_w range of 8.8–9.0. Slip values were chosen as typical for earthquakes of this size; Witter et al. (2016) and Nicolsky et al. (2016) both use 10 m for simulating tsunamis to Stardust Bay and the Dutch Harbor tide gauge.

RMS values for sites 4–18 were lowest for models with slip in row C, and for sites 7–18 in both B and C (Table 2). However, models with the most number of sites between –25% and +25% difference of simulated to observed run-up typically had slip in row B (Table 2). Earthquakes with slip in the deeper subfaults (C and D) produced simulations with wider wavelength tsunamis and larger values of subsidence in the islands (Supplementary Fig. 4).

Pacific side of the IFM (sites 4–7): Simulated run-up was close to the ~15 m observed in the IFM for source models with 20 m slip in subfault A, but it was too high if 20 m slip was in subfaults B or C, or too small if in subfault D (Fig. 6). The only other scenario with good agreement to Pacific side sites was 10 m slip in both subfaults A and B or B and C. No model came close to matching the Concord Point site, potentially supporting the field hypothesis that the wrack line there reflected a geomorphically enhanced wave.

Bering side of the IFM (sites 8–10) and Dutch Harbor tide gauge (site 19): Very few simulations produced the 6–9 m of run-up observed on the Bering Sea side of the IFM. The best-fitting source models all had slip on the deepest subfault, subfault D (Fig. 6). To a large degree, however, these deeper ruptures fit observations better because of subsidence (up to 2 m) associated with these earthquakes (Supplementary Fig. 4). Similarly, the Dutch Harbor tide gauge recorded only a 0.69 m tsunami; thus the percent difference was sensitive to changes in earthquake-induced subsidence—models with slip in rows C or D tended to exceed observations here primarily because the site subsided during simulation.

Pacific eastern rupture (sites 11–18) and Scotch Cap (site 20): The tsunami at Cape Sagak behaved similarly to the

Table 2. Evaluation of simulated run-up percent differences from observed run-up. Smaller root-mean-square (RMS) values are more accurate models.

Source models	RMS for eastern sites 4–18	RMS for Pacific-facing sites 7–18	RMS for Kaua'i, Hawai'i, sites 21–22	No. sites (n = 18) where –25% to +25%
Johnson et al. (1994)	94%	94%	61%	0
Johnson + 20 in 15C	80%	78%	-	0
Johnson + 20 in 15D	85%	88%	-	0
Johnson + 20 in 16A	82%	77%	-	0
Johnson + 20 in 16B	75%	69%	-	0
Johnson + 40 in 16A	70%	63%	-	2
Johnson + 40 in 16B	60%	54%	-	4
20 m in A	53%	38%	20%	4
20 m in B	45%	33%	51%	6
20 m in C	41%	33%	58%	6
20 m in D	60%	67%	19%	3
20 m in A and B	50%	45%	54%	6
20 m in B and C	44%	44%	51%	4
20 m in C and D	39%	42%	61%	3
10 m in B	59%	47%	42%	4
10 m in A and B	57%	45%	13%	6
10 m in B and C	51%	40%	51%	6
10 m in A; 20 m in B	48%	39%	37%	4
10 m in B; 20 m in C	41%	35%	73%	4

https://doi.org/10.1017/qua.2018.39 Published online by Cambridge University Press

Pacific side of the IFM, with 20 m slip producing large run-up unless it was in the shallowest subfault A, and 10 m slip giving reasonably good results. Driftwood and Stardust Bays (sites 13 and 18) were similar to each other, with good agreement from 20 m slip in subfaults B and C, but a too small simulated tsunami from 10 m slip or 20 m slip in subfaults A or D (Fig. 6). No simulation came close to the observed run-up in the bay east of Riding Cove (site 16) or Scotch Cap (site 20) potentially because of bathymetric resolution problems discussed in the following section.

Kaua'i, Hawai'i (sites 21–22): Far-field simulations to Anahola and Hanalei on Kaua'i, Hawai'i, produce a tsunami with run-up on the order of the observations. Three source models were within ±25% of observations at both sites—10 m of slip on subfaults A and B, 20 m on subfault A, and 20 m on subfault D. Mid-depth rupture, in particular on subfault C, produced too large run-up in Hanalei, as did source models with 20 m slip on multiple subfaults. Interestingly, many cases with simulated run-up too high in Hanalei had run-up less than observed in Anahola.

DISCUSSION

Bathymetric problems

All of the sites on Bering side of the IFM, Nazan Cove, east of Riding Cove, Scotch Cap, and to some degree the splash at Concord Point on the Pacific side of the IFM proved problematic; few to no models were able to reach the observed run-up at these sites. Error in tsunami modeling is most commonly associated with bathymetric inaccuracy or too low bathymetric resolution (Pan et al., 2010; MacInnes et al., 2013). We consider the low-resolution 24 arc-second SAK bathymetry (refined to 4 arc-second resolution in our simulations) to be the primary cause of our model underestimations. Preferred resolution for modeling studies are on the order of 1 to 1/3 arc-second (Berger et al., 2011; Lynett et al., 2012; Arcos and LeVeque, 2015). The resolution of the SAK grid translates to one grid cell being 450 m and 750 m on a side. At such low resolution, the lack of details in the grid can cause run-up values to be either higher or lower, compared with observed results (MacInnes et al., 2013). Compared with reality, low-resolution bathymetry is oversimplified, each grid cell representing an average water depth, making the lower points higher and the higher points lower. This is a problem for the Bering side of the IFM because the passes between islands in the IFM are averaged to be shallower than in reality, which blocks much of the tsunami from passing through to the Bering side sites. The Concord Point splash, which at 60 m wide was smaller than a single grid cell in the SAK bathymetry, was not able to be reproduced because either the bathymetry did not have the detail necessary for the model to form a realistic representation of the coastal geometry or at our 4 arc-second resolution refinement, approximations in GeoClaw are not able to adequately reproduce highly complex tsunami flow patterns during shoaling and inundation at this site (Pan et al., 2010). The same can be said for the narrow valley east of Riding Cove. Finally, quantitatively evaluating the SAK and ETOPO1 bathymetries used in this study against nautical maps shows there are discrepancies, such as submarine features not present in bathymetry, simplification of offshore bathymetry, and shallower deep water passes near the IFM.

Large slip in the east

Comparison of all model results indicates that the magnitude of the 1957 Great Aleutian earthquake must have been closer to M_w 8.8–9.0 than the commonly accepted value of M_w 8.6. The observations of run-up between >10 m and 32 ± 2 m on the Pacific coasts of IFM, Umnak Island, Unalaska Island, and Sedanka Island spans 225 km. We can rule out a coseismic submarine landslide as the sole cause for the high run-up observations in a M_w 8.6 scenario because run-up was high throughout the eastern Aleutians. Our source models of Johnson et al. (1994) with local 20 or 40 m slip on only one subfault represented an isolated area of tsunami excitation, such as what a landslide would generate (Okal and Synolakis, 2004). The spatially restricted high tsunami from these source models agrees with what is known about tsunamis from or enhanced by submarine landslides elsewhere and hypothetically (Okal and Synolakis, 2004). A submarine landslide could locally enhance a wave on the adjacent island to high run-up elevations seen at a site, but not over all sites in the entire eastern rupture zone.

Extensive eastern high slip on the order of 10 to 20 m best reproduced the observed tsunami run-up heights. On the Pacific side of IFM (sites 4–7) 10 m slip source models were more accurate than those with 20 m slip; however, source models with 20 m slip produced better results at the other eastern Pacific locations (sites 11–18), suggesting that slip was likely higher near Unalaska. The models with 20 m slip in two subfault rows can be ruled out as being too large from results in the IFM (sites 4–10) and Hawai'i (sites 21–22). The lack of tsunami observations west of IFM precludes analysis and interpretation of slip in the western half of the rupture zone.

The depth of the slip in the eastern Aleutians is more elusive, but our results indicate that near 15 km is most likely. In the near field, source models with slip in rows B or C (15–26 km and 26–41 km depth on average) tended to be slightly better than those with slip in row A or D. However, Hawai'i sites can rule out subfault C (and B if slip is 20 m), as producing a too-high trans-Pacific tsunami. Although slip in row D resulted in simulations with good agreement to observations on the Bering-side near-field sites, it was because these models produced 1–2 m subsidence rather than a higher amplitude tsunami; such subsidence, however, was not observed. Slip on subfaults A (when 20 m) or A and B (10 m) both produced excellent results on Hawai'i. Therefore, in sum of all simulated sites, slip during 1957 was most likely greatest in subfault B, near the A to B transition (15 km). Nicolsky et al. (2016) similarly concluded that slip was less than 30 km, most likely in the 5–15 km range.

https://doi.org/10.1017/qua.2018.39 Published online by Cambridge University Press

Interplate coupling models based on GPS data show that the eastern 1957 rupture zone is freely slipping today close to the trench but is partially locked from 14 to 47 km depth adjacent to Umnak and Unalaska (Cross and Freymueller, 2008). If this pattern was similar prior to 1957, slip in our subfault B rather than A is more likely.

Implications for the local tsunami hazard

From an improved understanding of the 1957 Great Aleutian earthquake

The 1957 earthquake is recorded in earthquake databases as M_w 8.6 and M_t 9.0 (NOAA, NGDC, 2017). Both field observations and modeling support the large M_t, and we suggest that the earthquake's magnitude was closer to M_w 8.8–9.0, which would make it one of the largest earthquakes in the past century. If this earthquake is greater than M_w 8.6, it indicates the east-central Aleutian subduction zone can produce very large earthquakes. If, however, the seismic energy released was indeed M_w 8.6, then lower magnitude earthquakes, which statistically occur more frequently than higher magnitude events, are capable of producing oversized tsunamis from this subduction zone, increasing the tsunami risk (from more frequent earthquakes) for coastal communities in the Pacific.

Today's partial coupling of the mid-depth subduction zone (Cross and Freymueller, 2008) shows the region has future potential for another large slip event. Paleotsunamis from Stardust Bay (Witter et al., 2016) and the IFM confirm repeated large events as the past behavior for the region. Large slip in the east portends that the eastern half of the 1957 rupture zone released more strain accumulation than the west during rupture; thus future small postevent earthquakes, such as the 1985 M_w 8.0 and 1996 M_w 7.9 events in the western half (Johnson et al., 1994), can be considered less likely in the east.

From interdisciplinary work in the IFM

Aleuts living in the IFM would have experienced tsunamis. Our observations of (undated) paleotsunami deposits preserved in the IFM indicate a regular recurrence of large events. Paleotsunamis at Stardust Bay on Sedanka Island, dated to between 300–175, 660–560, 1170–1010, 1380–1280, and 1680–1510 cal yr BP (Witter et al., 2016), should be expected to have run-up in the IFM, the height of which depends on the western extension of their rupture areas. On average, this is a tsunami every 300–340 yr, with some longer and shorter intervals, during a time that the islands were occupied (Hatfield, V., Krylovich, O., Bruner, K., Okuno, M., Savinetsky, A., Vasyukov, D., West, D., unpublished manuscript). Potentially, the penultimate tsunami was a larger magnitude event than 1957, based on Butler et al.'s (2014) conclusion that a M_w 9.25 eastern Aleutian simulation was the most likely earthquake scenario to explain a tsunami deposit (dated as younger than 525–285 cal yr BP) in Makauawahi sinkhole on the island of Kaua'i in Hawai'i.

However, would the Aleut villages in the IFM have been destroyed by a tsunami? The 1957 tsunami wrack line did not reach the elevation of any archaeological site previously known or studied as part of the "Prehistoric Resilience in the Islands of Four Mountains" project. Bering-side archaeological sites were typically >30 m elevation (elevations in Hatfield, V., Krylovich, O., Bruner, K., Okuno, M., Savinetsky, A., Vasyukov, D., West, D., unpublished manuscript). Unless sourced from the north (from nonsubduction-zone events such as submarine landslides or volcanic eruptions), the Bering sites were protected from past tsunamis. On the Pacific side, the 1957 wrack-line tsunami came within 5 m of the lowest part of one site. Our simulations of up to M_w 9.0 earthquakes, with high slip adjacent to the IFM, show that these tsunamis could potentially have inundated this location, although unlikely the entire extent of the site.

CONCLUSIONS

Through applying modern tsunami wrack-line survey methods and field techniques to a historical event, we measured the run-up and inundation of the 1957 Great Aleutian tsunami. In the IFM, wrack lines from the tsunami indicated a maximum run-up of 18 m on the Pacific side and 9 m on the Bering side. South Cove, the only site in the IFM with paleotsunami deposits, preserved up to five possible paleotsunamis and a record of local natural hazards. Outside the IFM, additional wrack lines exceed 18 m on Umnak, Unalaska, and Sedanka Islands—up to 32 ±2 m on Unalaska east of Riding Cove. Using GeoClaw, an open-sourced tsunami model, we determined that for the 1957 tsunami to produce the observed wrack lines, the earthquake released at least two or more times the energy than M_w 8.6; more likely it was M_w 8.8–9.0. High slip is necessary in the eastern portion of the aftershock zone, on the order of 10–20 m at or near 15 km depth. Because field observations do not exist for the entire aftershock zone, and seismic and GPS data of the Aleutians are limited, the exact magnitude and depth is a nonunique solution.

The orientation of the Aleutian subduction zone creates a tsunami threat beyond local communities to countries throughout the Pacific Ocean. As characteristics of past earthquakes and dynamics of the subduction zone become better understood, the style of rupture and recurrence probability of the eastern Aleutian trench will become clearer. Paleotsunami deposits from Sedanka Island (Witter et al., 2016) and the island of Kaua'i (Butler et al., 2014), combined with new paleotsunami deposits from the IFM, suggest that run-up from Aleutian earthquakes like 1957 and 1946 must be considered in trans-Pacific tsunami hazard assessments. The modern survey, paleotsunami study, and modeling work presented here constitute an important step toward developing a comprehensive representation of the hazard and risk presented by the Aleutian subduction zone and how tsunamis have affected past communities in the Aleutian Islands and across the Pacific.

https://doi.org/10.1017/qua.2018.39 Published online by Cambridge University Press

ACKNOWLEDGMENTS

This material is based on work supported by the National Science Foundation under grant no. PLR-1301929 and by Central Washington University Graduate Studies. Lydia Loopesko, Kale Bruner, Anne Fulton, Tina Neal, and the Higman-McKittrick family provided field assistance. This manuscript was improved by editor Kirsten Nicolaysen and two anonymous reviewers.

SUPPLEMENTARY MATERIALS

To view supplementary material for this article, please visit https://doi.org/10.1017/qua.2018.39

REFERENCES

Abe, K., 1979. Size of great earthquakes of 1837–1974 inferred from tsunami data. *Journal of Geophysical Research: Solid Earth* 84, 1561–1568.

Aigner, J., 1977. Anangula: an 8,500 B.P. coastal occupation in the Aleutian Islands. *Quartär* 27/28, 65–102.

Amante, C., Eakins, B.W., 2009. ETOPO1 1 Arc-Minute Global Relief Model: Procedures, Data Sources and Analysis. National Oceanic and Atmospheric Administration (NOAA) Technical Memorandum NESDIS NGDC-24. NOAA, National Geophysical Data Center, Marine Geology and Geophysics Division, Boulder, CO.

Arcos, M.E.M., LeVeque, R.J., 2015. Validating velocities in the GeoClaw tsunami model using observations near Hawaii from the 2011 Tohoku tsunami. *Pure and Applied Geophysics* 172, 849–867.

Berger, M.J., George, D.L., LeVeque, R.J., Mandli, K.T., 2011. The GeoClaw software for depth-averaged flows with adaptive refinement. *Advances in Water Resources* 34, 1195–1206.

Black, R., 1974. Geology and ancient Aleuts, Amchitka and Umnak Islands, Aleutians. *Arctic Anthropology* 11, 126–140.

Black, R., 1975. Late-Quaternary geomorphic processes: effects on the ancient Aleuts of Umnak Island in the Aleutians. *Arctic* 28, 139–169.

Butler, R., Burney, D., Walsh, D., 2014. Paleotsunami evidence on Kaua'i and numerical modeling of a great Aleutian tsunami. *Geophysical Research Letters* 41, 6795–6802.

Butler, R., Frazer, L.N., Templeton, W.J., 2016. Bayesian probabilities for M_w 9.0+ earthquakes in the Aleutian Islands from a regionally scaled global rate. *Journal of Geophysical Research: Solid Earth* 121, 3586–3608.

Clawpack Development Team, 2014. Clawpack Software, Version 5.3.1 (accessed July 1, 2017). http://www.clawpack.org.

Cross, R.S., Freymueller, J.T., 2008. Evidence for and implications of a Bering plate based on geodetic measurements from the Aleutians and western Alaska. *Journal of Geophysical Research: Solid Earth* 113, B07405.

DeMets, C., Gordon, R.G., Argus, D.F., 2010. Geologically current plate motions. *Geophysical Journal International* 181, 1–80.

Freymueller, J.T., Woodard, H., Cohen, S., Cross, R., Elliott, J., Larsen, C., Hreinsdottir, S., Zweck, C., 2008. Active deformation processes in Alaska, based on 15 years of GPS measurements. In: Freymueller, J.T., Haeussler, P.J., Wesson, R., Ekström, G. (Eds.), Active Tectonics and Seismic Potential of Alaska. Geophysical Monograph 179. American Geophysical Union, Washington, DC, pp. 1–42.

Friday, D.Z., Taylor, L.A., Eakins, B.W., Carignan, K.S., Love, M. R., Grothe, P.R., 2012. Digital Elevation Model of Kauai, Hawaii: Procedures, Data Sources and Analysis. Prepared for the Pacific Marine Environmental Laboratory (PMEL) National Oceanic and Atmospheric Administration (NOAA) Center for Tsunami Research. NOAA, National Geophysical Data Center, Marine Geology and Geophysics Division, Boulder, CO.

Global Volcanism Program, Smithsonian Institution, 2013. Cleveland (311240). In: Venzke, E. (Ed.), Volcanoes of the World, v. 4.6.0 (accessed July 6, 2017). http://volcano.si.edu/volcano.cfm?vn=311240.

Goto, K., Hashimoto, K., Sugawara, D., Yanagisawa, H., Abe, T., 2014. Spatial thickness variability of the 2011 Tohoku-oki tsunami deposits along the coastline of Sendai Bay. *Marine Geology* 358, 38–48.

Griswold, F.R., La Selle, S., Richmond, B.M., Jaffe, B.E., Gelfenbaum, G.R., Chague-Goff, C., LeVeque, R.J., Bellanova, P., Sugawara, D., Nelson, A.R., 2016. Summary of paleotsunami investigations in Aliomanu, Anahola, Kauai. In: 2016 Fall Meeting. American Geophysical Union, San Francisco, CA, abstract no. NH43A-1815.

Hayes, G.P., Wald, D.J., Johnson, R.L., 2012. Slab1.0: a three-dimensional model of global subduction zone geometries. *Journal of Geophysical Research: Solid Earth* 117, B01302.

Higman, B., 2007. Parsing the Sandy Onshore Deposits of Modern Tsunamis. PhD dissertation, University of Washington, Seattle.

International Tsunami Survey Team (ITST). 2014. Post-tsunami Survey Field Guide. 2nd ed. IOC Manuals and Guides No. 37, UNESCO, Paris.

Johnson, J.M., Tanioka, Y., Ruff, L.J., Satake, K., Kanamori, H., Sykes, L.R., 1994. The 1957 Great Aleutian earthquake. *Pure and Applied Geophysics* 142, 3–28.

Kanamori, H., 1977. The energy release in great earthquakes. *Journal of Geophysical Research* 82, 2981–2987.

Kitamura, S., Kodaka, T., Kataoka, J., 1961. Geological survey on the Chile Earthquake Tsunami affected areas in the Sanriku coast, northeast Japan. [In Japanese with English abstract.] Contributions from the Institute of Geology and Palaeontology, Tohoku University 52, 1–40.

Lander, J.F., 1996. Tsunamis Affecting Alaska 1737–1996. National Oceanic and Atmospheric Administration, National Geophysical Data Center, Boulder, CO.

La Selle, S., Richmond, B., Arcos, M., Jaffe, B., Lunghino, B., Kane, H., Bishop, J., Habel, S., 2016. Searching for a paleotsunami record in the Hawaiian Islands. In, 2016 Fall Meeting. American Geophysical Union, San Francisco, CA, abstract no. NH34A-1820.

Laughlin, S., Laughlin, W., McDowell, M., 1975. Anangula Blade site excavations, 1972 and 1973. *Anthropological Papers of the University of Alaska* 17, 39–48.

LeVeque, R.J., George, D.L., Berger, M.J., 2011. Tsunami modeling with adaptively refined finite volume methods. *Acta Numerica* 20, 211–289.

Lim, E., Eakins, B.W., Wigley, R., 2011. Coastal Relief Model of Southern Alaska: Procedures, Data Sources and Analysis. National Oceanic and Atmospheric Administration (NOAA) Technical Memorandum NESDIS NGDC-43. NOAA, National Geophysical Data Center, Marine Geology and Geophysics Division, Boulder, CO.

Lynett, P., Weiss, R., Renteria, W., De La Torre Morales, G., Son, S., Arcos, M.E.M., MacInnes, B.T., 2012. Coastal impacts

of the March 11th Tohoku, Japan Tsunami in the Galapagos Islands. *Pure and Applied Geophysics* 170, 1189–1206.

MacInnes, B.T., Gusman, A.R., LeVeque, R.J., Tanioka, Y., 2013. Comparison of earthquake source models for the 2011 Tohoku event using tsunami simulations and near-field observations. *Bulletin of the Seismological Society of America* 103, 1256–1274.

MacInnes, B.T., Pinegina, T.K., Bourgeois, J., Razhigaeva, N.G., Kaistrenko, V.M., Kravchunovskaya, E.A., 2009. Field survey and geological effects of the 15 November 2006 Kuril tsunami in the middle Kuril Islands. In: Cummins, P.R., Satake, K., Kong, L.S.L. (Eds.), Tsunami Science Four Years after the 2004 Indian Ocean Tsunami. Birkhäuser, Basel, Switzerland, pp. 9–36.

Major, J.J., Pierson, T.C., Dinehart, R.L., Costa, J.E., 2000. Sediment yield following severe volcanic disturbance—a two-decade perspective from Mount St. Helens. *Geology* 28, 819–822.

Mandli, K.T., Ahmadia, A.J., Berger, M.J., Calhoun, D.A., George, D.L., Hadjimichael, Y., Ketcheson, D.I., Lemoine, G.I., LeVeque, R.J., 2016. Clawpack: building an open source ecosystem for solving hyperbolic PDEs. *PeerJ Computer Science* 2, e68.

Morton, R.A., Gelfenbaum, G., Jaffe, B.E., 2007. Physical criteria for distinguishing sandy tsunami and storm deposits using modern examples. *Sedimentary Geology* 200, 184–207.

National Oceanographic and Atmospheric Administration (NOAA), 2017. Nikolski, AK - Station ID: 9462450 (accessed July 2017). https://tidesandcurrents.noaa.gov/stationhome.html?id=9462450.

National Oceanographic and Atmospheric Administration (NOAA), National Geophysical Data Center (NGDC), 2017. NGDC/WDS Global Historical Tsunami Database (accessed July 2017). https://www.ngdc.noaa.gov/hazard/tsu_db.shtml.

Nicolsky, D.J., Freymueller, J.T., Witter, R.C., Suleimani, E.N., Koehler, R.D., 2016. Evidence for shallow megathrust slip across the Unalaska seismic gap during the great 1957 Andreanof Islands earthquake, eastern Aleutian Islands, Alaska. *Geophysical Research Letters* 43, 10328–10337.

Okada, Y., 1985. Surface deformation due to shear and tensile faults in a half-space. *Bulletin of the Seismological Society of America* 75, 1135–1154.

Okal, E.A., Synolakis, C.E., 2004. Source discriminants for near-field tsunamis. *Geophysical Journal International* 158, 899–912.

Oliver, J., Murphy, L., 1971. WWNSS: seismology's global network of observing stations. *Science* 174, 254–261.

Pan, W., Wang, S., Cai, S., 2010. Numerical simulations of the coastal effects of tsunami waves caused by the 1993 Hokkaido-Nansei-Oki earthquake. *Chinese Journal of Oceanology and Limnology* 28, 1029–1039.

Peterson, J.R., Hutt, C.R., 2014. World-Wide Standardized Seismograph Network: A Data Users Guide. Open-File Report 2014-1218. U.S. Geological Survey, Reston, VA.

Ramalho, R.S., Quartau, R., Trenhaile, A.S., Mitchell, N.C., Woodroffe, C.D., Ávila, S.P., 2013. Coastal evolution on volcanic oceanic islands: a complex interplay between volcanism, erosion, sedimentation, sea-level change and biogenic production. *Earth-Science Reviews* 127, 140–170.

Ryan, H.F., von Huene, R., Wells, R.E., Scholl, D.W., Kirby, S., Draut, A.E., 2012. History of earthquakes and tsunamis along the eastern Aleutian-Alaska megathrust, with implications for tsunami hazards in the California continental borderland. *U.S. Geological Survey Professional Paper* 1795-A, 1–31.

Salsman, G.G., 1959. The Tsunami of March 9, 1957, as Recorded at Tide Stations. U.S. Department of Commerce, Coast and Geodetic Survey, Technical Bulletin No. 6. U.S. Government Printing Office, Washington, DC.

Scott, W.E., Nye, C.J., Waythomas, C.F., Neal, C.A., 2010. August 2008 eruption of Kasatochi volcano, Aleutian Islands, Alaska—resetting an island landscape. *Arctic, Antarctic, and Alpine Research* 42, 250–259.

Strover, C.W., Coffman, J.L., 1993. Seismicity of the United States, 1568-1989 (Revised). U.S. Geological Survey (USGS) Professional Paper 1527. USGS, Denver, CO.

Sykes, L.R., Kisslinger, J.B., House, L., Davies, J.N., Jacob, K.H., 1980. Rupture zones of great earthquakes in the Alaska-Aleutian arc, 1784 to 1980. *Science* 210, 1343–1345.

Wesson, R.L., Boyd, O.S., Mueller, C.S., Bufe, C.G., Frankel, A.D., Petersen, M.D., 2007. Revision of Time-Independent Probabilistic Seismic Hazard Maps for Alaska. Open-File Report 2007-1043. U.S. Geological Survey, Reston, VA.

Witter, R., Briggs, R., Koehler, R., Gelfenbaum, G., Engelhart, S., Nelson, A., Carver, G., Bender, A., Hemphill-Haley, E., 2014. Evidence for high tsunamis in the Fox Islands implies repeated Aleutian megathrust earthquakes in the Unalaska seismic gap. In: *Seismological Research Letters*, Vol 85. Seismological Society of America Annual Meeting, Anchorage, AK, pp. 441.

Witter, R.C., Carver, G.A., Briggs, R.W., Gelfenbaum, G.R., Koehler, R.D., La Selle, S., Bender, A.M., Englehart, S.E., Hemphill-Haley, E., Hill, T.D., 2016. Unusually large tsunamis frequent a currently creeping part of the Aleutian megathrust. *Geophysical Research Letters* 43, 76–84.